



Titre: Impacts of Continuous Inflow of Low Concentrations of Silver Nanoparticles on Biological Performance and Microbial Communities of Aerobic Heterotrophic Wastewater Biofilm
Title:

Auteurs: Sanaz Alizadeh, Arshath Abdul Rahim, Bing Guo, Jalal Hawari, Subhasis Ghoshal, & Yves Comeau
Authors:

Date: 2019

Type: Article de revue / Article

Référence: Alizadeh, S., Abdul Rahim, A., Guo, B., Hawari, J., Ghoshal, S., & Comeau, Y. (2019). Impacts of Continuous Inflow of Low Concentrations of Silver Nanoparticles on Biological Performance and Microbial Communities of Aerobic Heterotrophic Wastewater Biofilm. *Environmental Science & Technology*, 53(15), 9148-9159. <https://doi.org/10.1021/acs.est.9b01214>
Citation:

 **Document en libre accès dans PolyPublie**
Open Access document in PolyPublie

URL de PolyPublie: <https://publications.polymtl.ca/9089/>
PolyPublie URL:

Version: Version finale avant publication / Accepted version
Révisé par les pairs / Refereed

Conditions d'utilisation: Tous droits réservés / All rights reserved
Terms of Use:

 **Document publié chez l'éditeur officiel**
Document issued by the official publisher

Titre de la revue: Environmental Science & Technology (vol. 53, no. 15)
Journal Title:

Maison d'édition: ACS Publications
Publisher:

URL officiel: <https://doi.org/10.1021/acs.est.9b01214>
Official URL:

Mention légale: This document is the Accepted Manuscript version of a Published Work that appeared in final form in *Environmental Science & Technology* (vol. 53, no. 15), copyright © American Chemical Society after peer review and technical editing by the publisher. To access the final edited and published work see <https://doi.org/10.1021/acs.est.9b01214>
Legal notice:

6 **Abstract**

7 In this study, two bench-scale moving bed biofilm bioreactors (MBBRs), achieving soluble
8 organic matter removal, were exposed to 10.9 and 109 $\mu\text{g/L}$ polyvinylpyrrolidone (PVP)-coated
9 AgNPs for 9 weeks (64 d). Distribution of continuously added AgNPs were characterized in
10 influent, bioreactor and effluent of MBBRs using single-particle inductively coupled plasma
11 mass spectroscopy (spICP-MS). Continuous exposure to both AgNP_{inf} concentrations
12 significantly decreased soluble chemical oxygen demand (S_{COD}) removal efficiency (11% to
13 31%) and reduced biofilm viability (8% to 30%). Specific activities of both intracellular
14 dehydrogenase (DHA) and extracellular α -glucosidase (α -Glu) and protease (PRO) enzymes
15 were significantly inhibited (8% to 39%) with an observed NP dose-dependent intracellular
16 reactive oxygen species (ROS) production and shift in biofilm microbial community composition
17 by day 64. The release of significant mass of Ag via effluent (<78%), dominantly in NP form
18 due to the limited retention capacity of aerobic heterotrophic biofilm, provide new and useful
19 insight into fate of AgNPs in biofilm-laden engineered biological systems and their
20 corresponding inhibitory effects at environmentally representative NP concentrations maintained
21 over an extended period. To our knowledge, this is the first study evaluating chronic inhibitory
22 effect of AgNPs on attached-growth wastewater process efficiency and its microbial
23 communities at representative environmental AgNP concentrations by combining biological
24 response and NP characterization.

25

26

27

28 **1. Introduction**

29 Engineered nanoparticles (ENPs) are manufactured at an estimated rate of 11.5 million tons per
30 year for various industrial and commercial applications¹. Silver nanoparticles (AgNPs) are
31 predominantly used as antimicrobial agents in commercial products, cosmetics, food processing
32 and water industries¹. This rapidly developing nanotechnology market, however, is leading to
33 their environmental exposure, with a significant fraction of the AgNP-laden domestic and
34 industrial waste streams being released in municipal water resource recovery facilities (WRRFs)
35 at an estimated influent concentration ranging from 10 ng/L to 1.5 $\mu\text{g/L}$ ²⁻⁴. Thus, WRRFs serve as
36 a key interface between ENPs releases and their environmental distribution into downstream
37 ecosystems. Previous studies on the inhibitory effects of AgNPs (0.1 to 50 mg/L) in suspended-
38 growth systems showed adverse effects on the biological performance and biomass activity
39 caused by oxidative stress, cell membrane damage and inactivation of key enzymes at sufficient
40 AgNP doses ($< 1 \text{ mg/L}$)⁵⁻⁹. Yet, the interaction between biofilm processes and ENPs including
41 AgNPs are poorly understood.

42 Attached growth processes, such as moving bed biofilm reactors (MBBRs), are commonly used
43 as an upgrade or replacement for existing biological processes to meet current and new effluent
44 discharge requirements, while minimizing plant footprint and operating costs^{10,11}. In 2014, more than
45 1200 WRRFs in at least 50 countries utilize the MBBR technology in both the municipal and
46 industrial sectors with over 36 in North America^{12,13}. A limited number of studies investigated
47 the impact of a single dose of AgNPs (1 to 200 mg/L) over 24 to 96 h, using mono-species
48 biofilms, particularly *P. putida* based biofilms or wastewater biofilms in simplified biological
49 media^{11,14-16}. Their findings indicated higher potential of biofilm bacteria than planktonic bacteria
50 to withstand the toxic effects of AgNPs, primarily due to the presence of extracellular polymeric
51 substances (EPS), the primary components of biofilm¹⁵, which act to reduce AgNP diffusion in

52 biofilms¹⁷ over short term exposure conditions. Yet, the results of short-term exposure studies
53 may fail to capture the effects of the expected accumulation of AgNPs and higher mass transport
54 of AgNPs by diffusion into deeper layers of the biofilm over extended time intervals, thus
55 underestimating the potential toxicity of AgNPs over long-term exposure scenarios^{18,19}. Further
56 research is thus required first, to understand the interaction mechanisms between ENPs and
57 mature, mixed culture wastewater biofilms and second, to investigate the corresponding AgNP-
58 induced inhibitory effects at environmentally representative NP concentrations under conditions
59 that are representative of typical WRRF processes.

60 Rigorous physical and chemical characterization of AgNPs combined with extensive biological and
61 toxicological evaluations in WRRFs are critical in laying the grounds for a better understanding
62 of their environmental fate and for the design of better alternative treatment strategies and future
63 regulations²⁰. The current understanding of the environmental fate and transformation of ENPs is
64 limited due to the limitations of ENP characterization techniques in complex environmental
65 matrices containing ENPs at very low, environmentally relevant concentrations^{21,22}. Single-
66 particle inductively coupled plasma–mass spectrometry (spICP-MS) is an emerging powerful
67 technique with the potential to address such limitations, providing quantitative characterization
68 of metal NP size distributions, particle number concentrations and dissolved metal
69 concentrations at low NPs concentrations in complex, organic matter-rich, environmental
70 matrices such as wastewaters²³⁻²⁵.

71 In this study, we investigated the impact of continuous injection of low concentrations of AgNPs
72 in an attached growth wastewater treatment process using aerobic heterotrophic wastewater
73 biofilms at nominal influent concentrations of 10.9 and 109 $\mu\text{g/L}$ AgNPs to approximate
74 environmentally relevant concentrations of AgNPs. Although, these concentrations would still be

75 at the higher end of the estimated concentration for WRRFs, they would mimic a worst case
76 scenario such as release from biosolid-treated soil or landfills by flooding events or production
77 plant discharge²⁶. The specific objectives of this study were (1) to characterize the interactions
78 and distribution of AgNPs in a biofilm-laden wastewater biological process and (2) to determine
79 the impact of AgNPs on primary biological functions and microbial community of wastewater
80 biofilms. Two bench-scale MBBRs were operated for organic matter removal and were fed with
81 a synthetic soluble influent representative of a municipal wastewater. The impacts of AgNPs on
82 the performance of the MBBRs were characterized by monitoring several performance indicators
83 including S_{COD} removal efficiency, effluent quality and enzymatic activity over a 9-week (64 d)
84 exposure period.

85 The biological responses of aerobic heterotrophic biofilm were characterized in terms of
86 (i) biofilm cell membrane integrity using DNA-binding stains, (ii) AgNP-mediated oxidative
87 stress via intracellular ROS measurement and (iii) microbial metabolic functions by intracellular
88 DHA and extracellular α -Glu and PRO specific enzymatic activities using colorimetric assays.
89 The biofilm microbial community compositions, at both influent AgNPs concentrations, were
90 characterized through high-throughput sequencing. The aggregation state, dissolution and
91 distribution of AgNPs were determined between different reactor components (i.e. influent,
92 bioreactor and effluent) using spICP-MS techniques and transmission electron microscopy with
93 energy dispersive X-ray spectroscopy (TEM EDS). To the best of our knowledge, this is the first
94 study evaluating the long-term inhibitory effect of AgNPs on attached-growth wastewater
95 process efficiency and its microbial communities at environmentally relevant AgNP
96 concentrations ($< 100 \mu\text{g/L}$ AgNPs) by combining biological responses and the NP distribution,
97 characterization and Ag speciation data.

98 2. Methods

99 2.1 Reactor configuration and AgNPs exposure

100 Two 1 L bench-scale MBBRs, achieving organic matter removal at a hydraulic retention time
101 (HRT) of 3 hours, operated in parallel under identical conditions, were fed a synthetic soluble
102 influent (Table S1) to ensure constant influent characteristics and well-controlled conditions to
103 characterize the inhibitory effects of the PVP-AgNPs. The concentrated synthetic wastewater
104 (1.3 ± 0.2 g S_{COD}/L) was pumped and diluted with tap water before entering the reactors to
105 obtain an influent COD concentration of 655 ± 6 mg S_{COD}/L at an organic loading rate of $11 \pm$
106 0.2 g COD $\text{m}^{-2} \text{d}^{-1}$ of active surface area to be representative of the soluble fraction of a medium
107 to high strength domestic wastewater with typical COD/TKN/TP ratio of 100/12.0/2.0²⁷. The
108 characteristics of the synthetic influent (Table S2) and detailed reactor operation conditions are
109 presented as supplementary information (SI). After reaching quasi steady-state conditions with a
110 stable S_{COD} removal efficiency, the reactors were monitored for 85 days as a control period.
111 Influent AgNP suspensions were prepared by dilution of 50 nm PVP-coated AgNPs stock
112 suspension (4.73 mg/mL, Nanocomposix Inc., San Diego, US) in Milli-Q water. The zeta
113 potential and surface area of AgNPs were -37.8 mV (at pH 4) and 9.8 m^2/g , respectively, based
114 on the AgNP product description, with a mean diameter of 48 ± 2 nm (SpICP-MS, PerkinElmer
115 NexION 300X). The AgNP influent suspensions were pumped to each reactor from day 125 at a
116 constant flow rate (2.7 ± 0.1 mL/min), resulting in an average influent total Ag concentration of
117 14 ± 0.5 $\mu\text{g}/\text{L}$ Ag for MBBR₁ and 130 ± 14 $\mu\text{g}/\text{L}$ Ag for MBBR₂ after dilution. The influent
118 nanoparticle suspensions were replenished every 24 h. The effluent water quality, biofilm
119 biological responses (e.g. viability or enzyme activity) and Ag distribution were monitored over
120 64 days. Chemical oxygen demand (COD), total suspended solids (TSS) and volatile suspended
121 solids (VSS) were measured according to Standard Methods²⁸.

122 2.2 Silver analyses

123 The influent, bioreactor and effluent were sampled every 24 h over the first week (day 125-130)
124 and every 3 days afterwards (day 133-189) for a total period of 9 weeks (Figure S1). Bioreactor
125 and effluent samples contained suspended flocs (145 to 480 mg TSS/L) but no K5 carriers. Total
126 Ag concentration was measured in acid-digested homogenized samples using a PerkinElmer
127 NexION 300x ICP-MS in standard mode as described in our previous study¹⁹. The homogenized
128 samples were allowed to settle for about 30 to 45 s and the aqueous supernatant was collected.
129 AgNP concentration and size as well as dissolved Ag were determined simultaneously using
130 spICP-MS, supported by Syngistix nano application module (version 1.1) as described by Azodi
131 et al.²³. Instrumental and data acquisition parameters of the analysis are indicated in SI (Table
132 S3). A cumulative Ag mass distribution in influent ($M_{Ag, inf}$), bioreactor ($M_{Ag, bio}$) and effluent ($M_{Ag, eff}$)
133 of each MBBR was calculated based on the corresponding total Ag concentrations,
134 obtained from ICP-MS analysis, influent and effluent flow rates, and volume of the bioreactor
135 for each time interval (Δt) as described in our previous study¹⁹. Ag fractionation and the detailed
136 equations and Ag mass balance are presented in SI.

137 2.3 Viability and key enzymatic activities of attached biofilm

138 Bacterial viability of attached biofilms was evaluated using the Live/Dead *BacLight* bacterial
139 viability kit (Molecular Probes, Invitrogen, Kit L13152) and a micro plate reader (Synergy-HT,
140 BioTek, USA) as described by Chen et al.²⁹. The specific activities of DHA, α -Glu and PRO
141 enzymes were measured by a colorimetric method^{30,31} using 0.5% 2-(4-iodophenyl)-3-(4-
142 nitrophenyl)-5-phenyl-2H-tetrazolium chloride (INT), 1% *p*-nitrophenyl α -D-glucopyranoside
143 and 0.5% azocasein, respectively, as a substrate for the reactions. The intracellular ROS
144 production, as an indicator of oxidative stress, was determined using dichlorodihydrofluorescein

145 diacetate (H₂DCF-DA, Molecular Probes, Invitrogen)³². H₂-DCFDA was used as a cell-permeant
146 reagent that measures hydroxyl, peroxy and other reactive oxygen species activity in cells.
147 Details regarding all enzyme activity and ROS assays are provided in SI.

148 **2.4 DNA Extraction, sequencing and microbial community analysis**

149 Biofilm samples were collected from MBBR₁ and MBBR₂ at the end of the control period
150 (MBBR₁^C, MBBR₂^C) and after exposure to AgNPs for 64 days (MBBR₁⁶⁴, MBBR₂⁶⁴). For each
151 set of the microbial community data, 10 carriers were selected randomly from each reactor; the
152 retained biofilm was homogenized and used for DNA extraction. Genomic DNA was extracted
153 from the biofilm samples using FastDNA[®]spin kit (MP Biomedicals, Santa Ana, CA) following
154 the manufacturer's instructions, and sent for library preparation and sequencing on the Illumina
155 Miseq PE250 platform at McGill University and Génome Québec Innovation Centre (Montréal,
156 Québec). Bacterial universal primers 515F (5'-GTGCCAGCMGCCGCGGTAA-3') and 806R
157 (5'-GGACTACHVGGGTWTCTAAT-3') were used to amplify the V4 variable region of the 16S
158 rDNA. Bioinformatics analysis was performed using QIIME2 pipelines. The de-multiplexed
159 forward and reverse sequences were quality-filtered using DADA2³³ at 100% sequence
160 similarity. Taxonomy was assigned using the 99% operational taxonomic unit (OTU) similarity
161 in the GreenGenes reference database. Alpha-diversity, beta-diversity and their statistical tests
162 were analyzed in QIIME2. Principal coordinates analysis (PCoA) was constructed using
163 weighted UniFrac distance matrix. Heatmap was generated in R using the "gplots" package.

164 **2.5 Statistical analysis**

165 The statistical significance of differences between treatments ($p < 0.05$), before and after
166 exposure to AgNPs, was evaluated with one-way repeated measures ANOVA using Statistica
167 version 12 (StatSoft Inc., USA).

168 3. Results and discussion

169 3.1 Fate of AgNPs in MBBRs over 64 days

170 The influent of MBBR₁ and MBBR₂ contained an average concentration of $10.9 \pm 1.6 \mu\text{g/L}$
171 AgNP ($[\text{AgNP}_{\text{inf}}]$) and $109.3 \pm 10 \mu\text{g/L}$ AgNP_{inf}, with mean diameter (d_{mean}) of 49 ± 7 nm and
172 48 ± 2 nm, respectively, (Figure S2D), corresponding to a total Ag concentration ($[\text{Ag}_{\text{inf}}]$) of 14
173 $\pm 2 \mu\text{g/L}$ Ag $130 \pm 14 \mu\text{g/L}$ Ag in corresponding reactors (Figure 1A, B). Each of these quantities
174 was independently measured by spICP-MS and ICP-MS. SpICP-MS analyses showed less than
175 10% variation in dissolved Ag concentrations ($[\text{dissolved Ag}_{\text{inf}}]$), in influent NP stock solutions
176 of both reactors over time (Figure S2A, B). Three distinct trends (Phases) were observed for Ag
177 concentration profiles in both reactors over the 64-day Ag loading (Figure 1A, B). Phase I
178 corresponded to the first 15 days of AgNP loading (day 125-140) during which both reactors
179 accumulated Ag in response to the AgNP addition and reached a relatively stable Ag retention
180 efficiency (61% to 72% of $[\text{Ag}_{\text{inf}}]$). A major fraction of the released total silver ($[\text{Ag}_{\text{eff}}]$) (40% to
181 63%) was associated with total suspended solids in effluent (TSS_{eff}) in MBBRs. Effluent Ag
182 concentration as NP (AgNP_{eff}) in MBBR₁ (0.2 to $1.4 \mu\text{g/L}$) and MBBR₂ (2.9 to $5.5 \mu\text{g/L}$)
183 corresponded to approximately $10\% \pm 3\%$ of $[\text{Ag}_{\text{eff}}]$ and $16\% \pm 4\%$ of $[\text{Ag}_{\text{eff}}]$, respectively, over
184 Phase I. SpICP-MS analyses showed variations in $[\text{dissolved Ag}_{\text{eff}}]$ in the effluent supernatant
185 of MBBR₁ (0.2 to $2.6 \mu\text{g/L}$) and MBBR₂ (4.7 to $11.9 \mu\text{g/L}$) representing about 16% to 49% of
186 $[\text{Ag}_{\text{eff}}]$ as Ag^+ partially or completely complexed to dissolved organic carbon (DOC) (Figure 1A,
187 B). High concentration of dissolved oxygen ($6 \pm 0.2 \text{ mg/L}$) and pH of 7.2-7.5 in the MBBRs
188 provided thermodynamically favorable conditions for oxidation driven dissolution of AgNPs.
189 Generally, the mean diameter of AgNP_{eff} was up to 7 nm smaller than AgNP_{inf} , despite the
190 minor aggregation over 3 initial days of exposure (Figure 1C).

191 The magnitude of change in the diameters was small because of the short average residence time
192 of the AgNPs in the reactor. The particle size distribution of AgNP_{eff} had slightly higher
193 concentrations of smaller particles compared to AgNP_{inf} (Figure S3). The relatively high amount
194 of [dissolved Ag_{eff}] on certain days (e.g., day 133 in MBBR_1 and day 154 in MBBR_2) cannot be
195 accounted for the changes in particle diameters in the effluent. It is likely that detachment and
196 release of soluble complexes Ag from the biofilm/EPS matrix resulted in relatively high fraction
197 of [dissolved Ag_{eff}] relative to $[\text{Ag}_{\text{eff}}]$. The attached biofilm ($\text{Ag}_{\text{carrier}}$) retained about 60% to 71%
198 of cumulative mass of total Ag loading in the influent ($M_{\text{Ag}_{\text{inf}}}$) in MBBR_1 (0.88 mg Ag/m² of
199 carrier active surface) and MBBR_2 (10.3 mg Ag/m² of carrier active surface) by the end of
200 Phase I (day 140), indicating an initial high Ag biofilm retention capacity (Figure 1D, E). The
201 carrier active surface area represents the biofilm covered surface area.

202 Phase II started with a gradual increase of $[\text{Ag}_{\text{eff}}]$ which reached a maximum concentration of 8.9
203 $\pm 1.7 \mu\text{g/L}$ Ag in MBBR_1 and $118.6 \pm 1.5 \mu\text{g/L}$ Ag in MBBR_2 over 10 days (day 140 - 150)
204 decreasing the Ag retention efficiency significantly ($p < 0.05$) compared to Phase I due to
205 biofilm detachment (Figure S5). A larger fraction of $[\text{Ag}_{\text{eff}}]$ (20% to 37%) was detected as NPs
206 in the effluent supernatant of MBBR_1 (8.9 to 11.2 $\mu\text{g/L}$) and MBBR_2 (9.02 to 26.5 $\mu\text{g/L}$). The
207 [dissolved Ag_{eff}] in MBBR_1 and MBBR_2 represented about $22\% \pm 3\%$ of $[\text{Ag}_{\text{eff}}]$ (1.3 to 3.04
208 $\mu\text{g/L}$) and $25\% \pm 8\%$ of $[\text{Ag}_{\text{eff}}]$ (11.9 to 25.30 $\mu\text{g/L}$) respectively, in this phase (Figure 1A, B).
209 By the end of Phase II (day 150), the attached biofilm retained only about 44% to 54% of
210 cumulative $M_{\text{Ag}_{\text{inf}}}$ in MBBRs (Figure 1D, E), followed by a continuous decrease in retention
211 efficiency (Figure 1A, B). The virgin surface of the biofilm retained much AgNPs during Phase
212 I, likely due to interactions of hydrophobic PVP coatings of AgNPs with heterogeneous

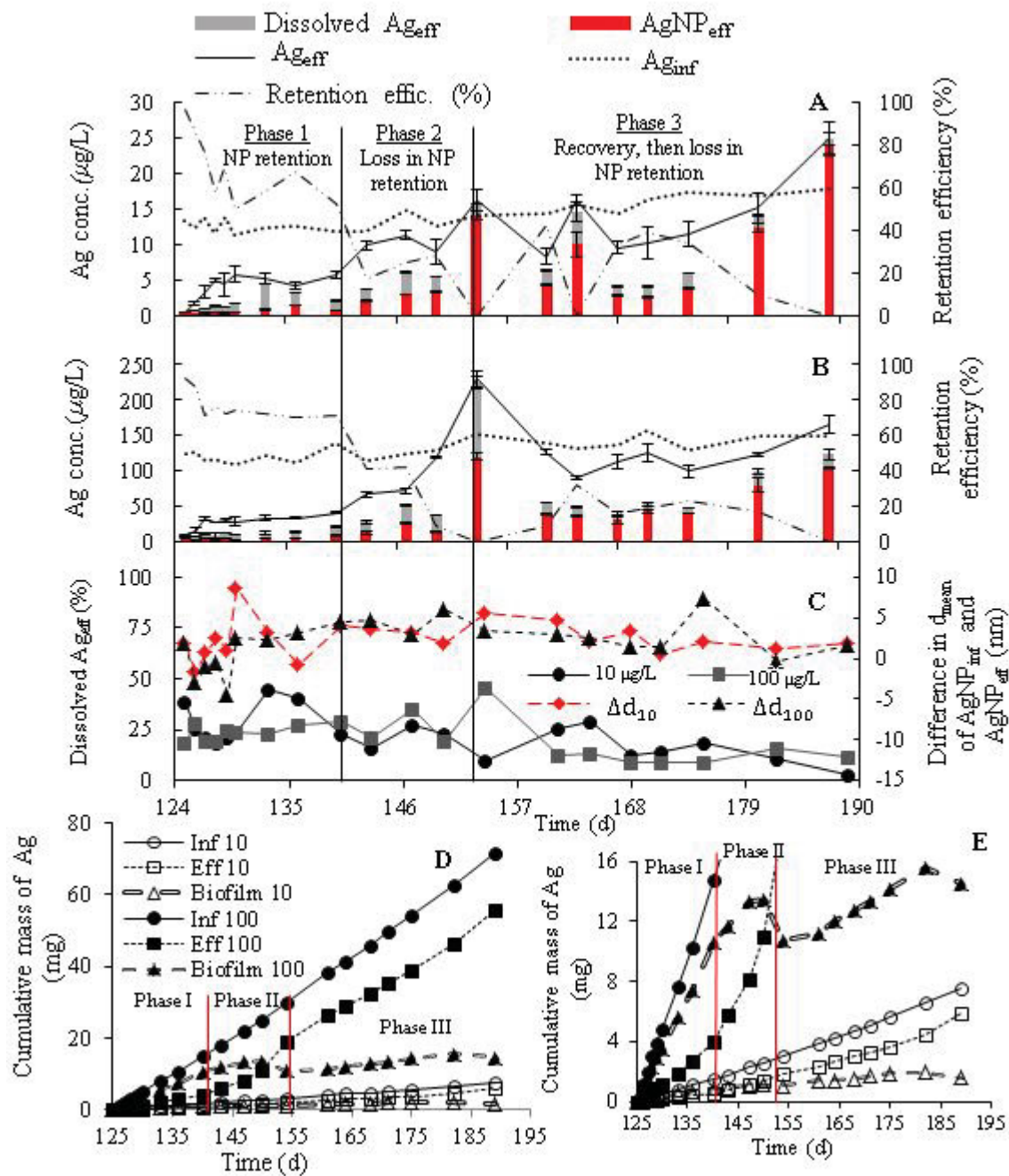
213 amphiphilic moieties of the biofilm surface³⁴. As the concentration of AgNPs increased inside
214 the reactors during Phase II, the local accumulation of PVP-AgNPs on the outer layer of the
215 biofilm must have blocked further deposition of AgNPs and caused decrease in NPs attachment
216 efficiency onto the biofilm surface³⁴.

217 Phase III corresponded to the period with Ag release and retention recovery events in both
218 reactors (day 154 - 189). The Ag distribution profile in MBBR₁ consisted of two Ag release
219 events on day 154 (week 4) and day 164 (week 6) with the [AgNP_{eff}] ($9.9 \pm 1.7 \mu\text{g/L}$ to $14.03 \pm$
220 $0.7 \mu\text{g/L}$) constituting 61% to 87% of detected [Ag_{eff}] (Figure 1A, C). Despite a slight Ag
221 recovery in retention by biofilm by day 175 (week 7), significantly higher [Ag_{eff}] were released
222 over the last two weeks of exposure, predominantly in the form of AgNPs (81% to 96% of [Ag_{eff}
223]) likely due to saturation of biofilm outer layers by AgNPs and/or biofilm sloughing off from
224 the surface of the carriers. MBBR₂ demonstrated a lower recovery for Ag retention over a longer
225 time interval as compared to MBBR₁ during the Phase III. A maximum Ag release of $229 \mu\text{g/L}$
226 Ag_{eff} was observed at the beginning of Phase III (day 154) in MBBR₂, with a dominant fraction
227 of [Ag_{eff}] detected as AgNP_{eff} (52% of [Ag_{eff}]) and dissolved Ag_{eff} (45% of [Ag_{eff}]) in the
228 aqueous phase of the effluent (Figure 1B), suggesting a saturation of the biofilm outer layers.
229 Thereafter, [AgNP_{eff}] (80 to $104 \mu\text{g/L}$) represented an average 40% to 65% of [Ag_{eff}] between
230 day 161 and day 189 (Figure 1B). A relatively smaller mass fraction of [Ag_{eff}] was accounted for
231 dissolved Ag_{eff} (11% to 15%) in both reactors in Phase III compared to Phases I and II
232 (Figure 1C). Attached biofilm retained less than 20% of cumulative M_{Ag_{inf}} in MBBR₁ (1.52 mg
233 Ag/m^2 of carrier active surface) and MBBR₂ (15.2 mg Ag/m^2 of carrier active surface),
234 respectively, and significant fraction of cumulative M_{Ag_{inf}} (> 78%) was released via the effluent
235 of the both reactors by the end of Phase III (day 189; Figure 1D, E), indicating poor retention

236 capacity of the biofilm over long term exposure. Similar high bioaccumulation of AgNPs¹¹ and
237 silica-coated iron oxide³⁵ in wastewater biofilms were reported at low NP concentrations over short-
238 term exposure whereas detachment of NP-rich biofilms became a source of NP-release as NP
239 concentrations increased over time.

240 A general conclusion from previous studies conducted in batch experiments³⁶, sequencing batch
241 reactors⁷, membrane bioreactors³⁷ and municipal WRRFs⁴ indicated an efficient AgNP removal
242 (72% to 95%) via accumulation in suspended growth activated sludge processes with no
243 extensive AgNP washout as shown here for the MBBRs. The quantitative characterization of
244 nanoparticles in MBBRs, using spICP-MS, indicated an initial adaptation of MBBR to silver
245 addition with an increase in total Ag release over time, predominantly in NP form, and a periodic
246 silver accumulation in biofilm coupled with a biomass concentration increase (Figure S4). Our
247 results imply that there is a limited retention capacity of aerobic heterotrophic biofilm for AgNPs
248 over a long time exposure, compared to the commonly studied activated sludge systems. The
249 observed decrease in [dissolved Ag_{eff}] over time in both MBBRs can be attributed to the
250 removal of Ag⁺ via their interaction with functional groups of macromolecules such as cysteine
251 and methionine in the EPS and biofilm matrix and their organic ligands, such as thiols^{38,39,40}.
252 Complete inhibition or significant decrease of AgNPs dissolution was reported in the presence of
253 Cl⁻ ions at low Cl/Ag ratios³⁹. We detected similar changes in the chemical composition of the
254 particles in the effluent of the MBBRs using TEM-EDS analysis (Figure S2). Similar
255 complexation of dissolved silver in wastewater effluents and their significantly reduced
256 bioavailability were reported for a 7 day-experiment⁴⁰. Azodi et al.²³ attributed the decrease in
257 dissolved Ag concentrations in the wastewater effluent to the reformation of the secondary NPs
258 from dissolved Ag.

259



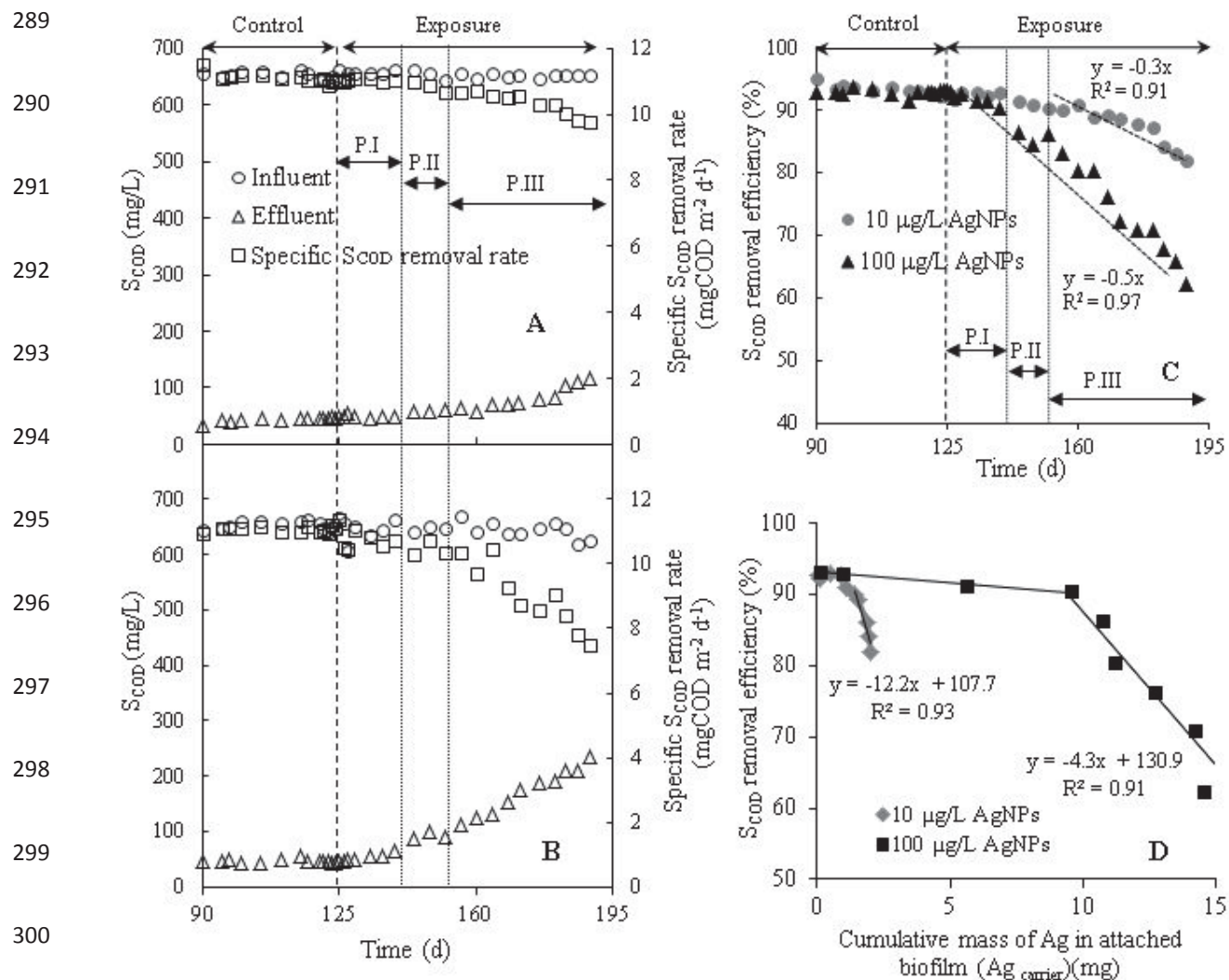
260

261 **Figure 1.** Fate and retention of Ag in MBBR receiving influent concentration of (A) $10 \mu\text{g/L}$
 262 AgNPs and (B) $100 \mu\text{g/L}$ AgNPs, (C) dissolution of AgNP_{eff} (%) and difference in mean
 263 diameter (d_{mean}) of AgNP_{inf} and AgNP_{eff} , (D) cumulative Ag mass distribution in influent (Inf),
 264 attached biofilm (Biofilm) and effluent (Eff) and (E) enlarged Y-scale of panel D.

265

266 3.2 Effects of AgNPs on the biological performance of a heterotrophic aerobic biofilm

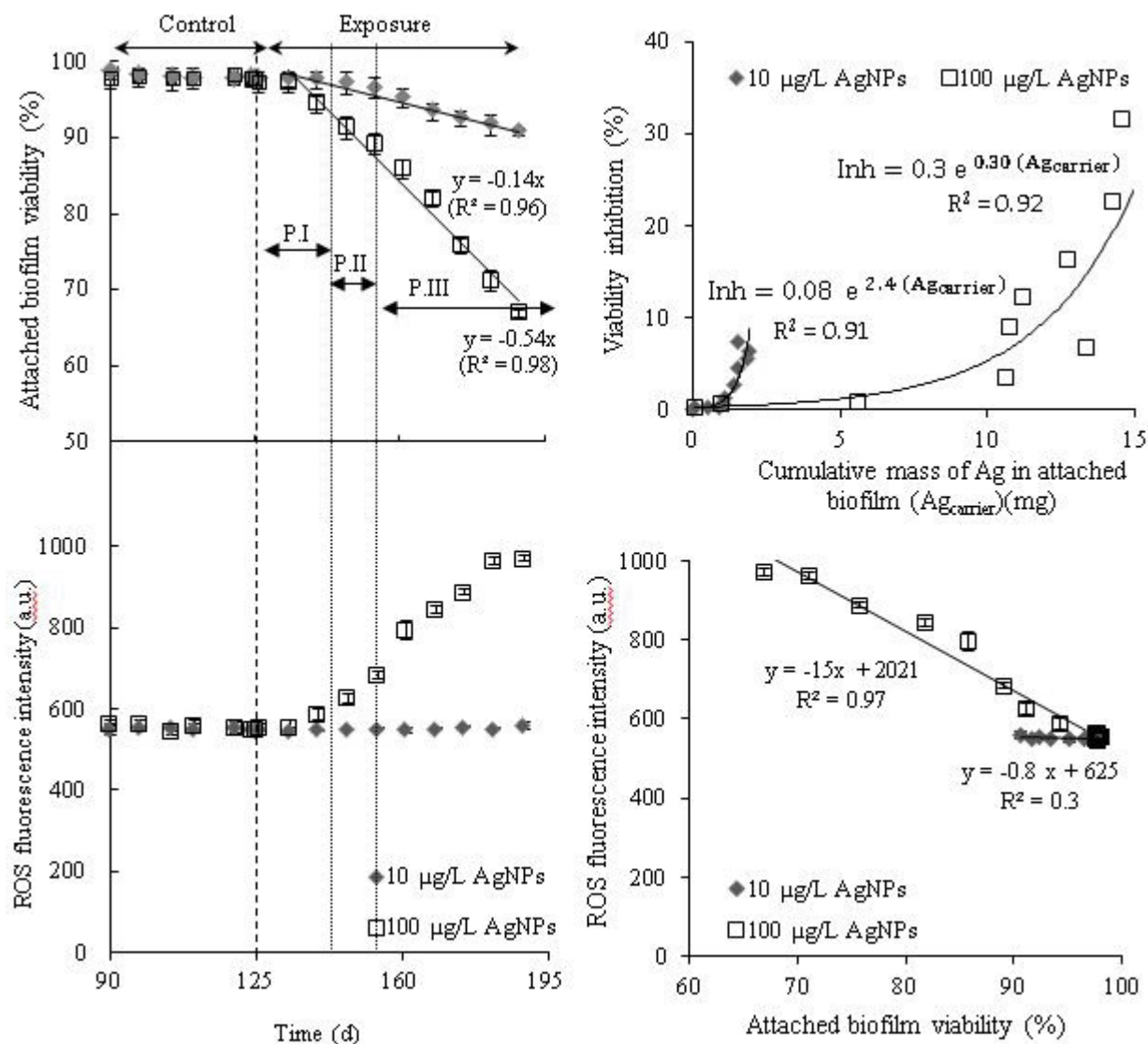
267 The biofilm-mediated S_{COD} removal efficiency was determined in the two MBBRs in response to
268 the 64-day continuous exposure to $[\text{AgNP}_{\text{inf}}]$ of 10.9 and 109 $\mu\text{g/L}$ (Figure 2A, B). Prior to
269 exposure to the AgNPs, both reactors consisted of $98\% \pm 0.2\%$ viable biofilm over the control
270 period (day 90-124) (Figure 3A) which stabilized the S_{COD} removal efficiency at 93% under
271 quasi steady state conditions (Figure 2A-C). The biodegradation of S_{COD} remained stable, after
272 injection of AgNPs, with an average S_{COD} removal efficiency of $92\% \pm 0.7\%$ over the first 35
273 days (day 125-161) in MBBR₁ and $91\% \pm 2\%$ over 23 days (day 125-147) in MBBR₂ indicating
274 an unperturbed primary phase (Figure 2C) with relatively stable biofilm viability ($> 96\%$)
275 (Figure 3A). Measured AgNP concentrations in MBBR₁ (0.16 to 0.60 $\mu\text{g/L}$ AgNP_{bio}) and
276 MBBR₂ (0.7 to 5.02 $\mu\text{g/L}$ AgNP_{bio}) and their corresponding dissolved Ag_{bio} of 0.3 to 1.2 $\mu\text{g/L}$
277 and 1.5 to 8.4 $\mu\text{g/L}$, respectively, over Phase I (Figure S2) were much lower than previously
278 reported threshold concentrations for toxicity of AgNPs and dissolved Ag for biofilms ($\text{IC}_{50, \text{PVP-}}$
279 $\text{AgNP@48h} = 114 \mu\text{g/L}$ and $\text{IC}_{50, \text{Ag+@48h}} = 44 \mu\text{g/L}^{41}$). As AgNP concentrations increased in reactors
280 (Figure S2C, D), a secondary phase was observed with higher numbers of inactivated cells,
281 resulting in significant inhibition of viable attached biofilm in MBBR₁ (8%) and MBBR₂ (31%)
282 by day 189 (Figure 3A). The S_{COD} removal efficiency significantly decreased ($p < 0.05$) by about
283 11% over 29 days (day 160-189) in MBBR₁, and by 31% after 41 days (day 133-189) in MBBR₂
284 (Figure 2C), corresponding to the observed patterns in Ag_{bio} and Ag_{eff} time profiles. Exposure to
285 both AgNP_{inf} concentrations also induced biofilm detachment from the surface of the carriers,
286 corresponding to the significant increase of TSS_{eff} (Figure S5). Significant detachment of
287 wastewater biofilm and concurrent release of accumulated AgNPs were similarly reported at
288 environmentally relevant AgNPs concentrations (22 and 105 $\mu\text{g/L}$ AgNPs)¹¹.



301 **Figure 2.** Effect of PVP-AgNPs addition on MBBR performance at (A) 10 μg/L AgNPs (B)
 302 100 μg/L AgNPs, (C) S_{COD} removal efficiency and (D) correlation between $Ag_{carrier}$ and S_{COD}
 303 removal efficiency (error bars are only shown when larger than symbol size). Note: P.I-III refers
 304 to three observed phases in Ag distribution profile.

305
 306 The inhibitory effect of AgNPs on both the S_{COD} removal efficiency (Figure 2D) and the biofilm
 307 viability inhibition (Figure 3B) were highly correlated ($0.91 < R^2 < 0.97$) to the retained mass of
 308 Ag in the carriers ($Ag_{carrier}$). High biomass surface area/volume ratio in attached growth
 309 processes (e.g. MBBR) enhances the deposition rate of AgNPs to attached biomass over time,
 310 leading to enhanced Ag retention per unit weight of biomass in MBBR. Thus, significant
 311 accumulation and associated mass transport of AgNPs into deeper layers of the biofilm can lead

312 to extensive spatial distribution of AgNPs in the biofilm cells, delivering toxic Ag^+ directly to
 313 adherent cells via interfacial dissolution of the surface-bound AgNPs and/or partly via direct
 314 uptake, leading to an enhanced time exposure and greater toxicity⁴².



315
 316 **Figure 3.** Effect of continuous PVP-AgNP injection on (A) attached cell viability, (B)
 317 intracellular ROS generation, (C) correlation between $\text{Ag}_{\text{carrier}}$ and attached biofilm viability
 318 inhibition and (D) correlation between viability inhibition and intracellular ROS generation
 319 (error bars are only shown when larger than symbol size). Note: P.I-III refers to three observed
 320 phases in Ag distribution profile.

321

322 Intracellular ROS did not significantly change in MBBR₁ (10.9 $\mu\text{g/L AgNP}_{\text{inf}}$), whereas its
323 concentration increased significantly (1.78-fold, $p < 0.05$) in MBBR₂ (109 $\mu\text{g/L AgNP}_{\text{inf}}$) over 64
324 days (Figure 2C), consistent with reported concentration-dependent ROS production in activated
325 sludge³². No correlation between biofilm viability inhibition and ROS production was observed
326 in MBBR₁ whereas the cell membrane integrity damage was highly correlated to increased ROS
327 generation in MBBR₂ ($R^2 = 0.97$) (Figure 3D), indicating both ROS-mediated and ROS-
328 independent effects of AgNPs on cell membrane integrity³². The interaction between AgNPs/Ag⁺
329 and the functional groups of proteins, involved in the cell respiratory chain, can lead to
330 intracellular ROS production. Biofilm was able to regulate the ROS production at lower AgNP
331 concentrations (1.4 to 9.04 $\mu\text{g/L AgNP}_{\text{bio}}$), likely via ROS scavenging enzymes (e.g. superoxide
332 dismutase)⁴³, higher concentrations of AgNPs in MBBR₂ (10.3 to 46.2 $\mu\text{g/L AgNP}_{\text{bio}}$), however,
333 caused significant overproduction of ROS which can overwhelm the antioxidant systems and
334 induce oxidative damage to cell membranes by for example modification of the unsaturated fatty
335 acids of the membrane phospholipids⁴⁴.

336 **3.3 Inhibitory effect of AgNPs on key enzymatic activities of aerobic heterotrophic biofilm**

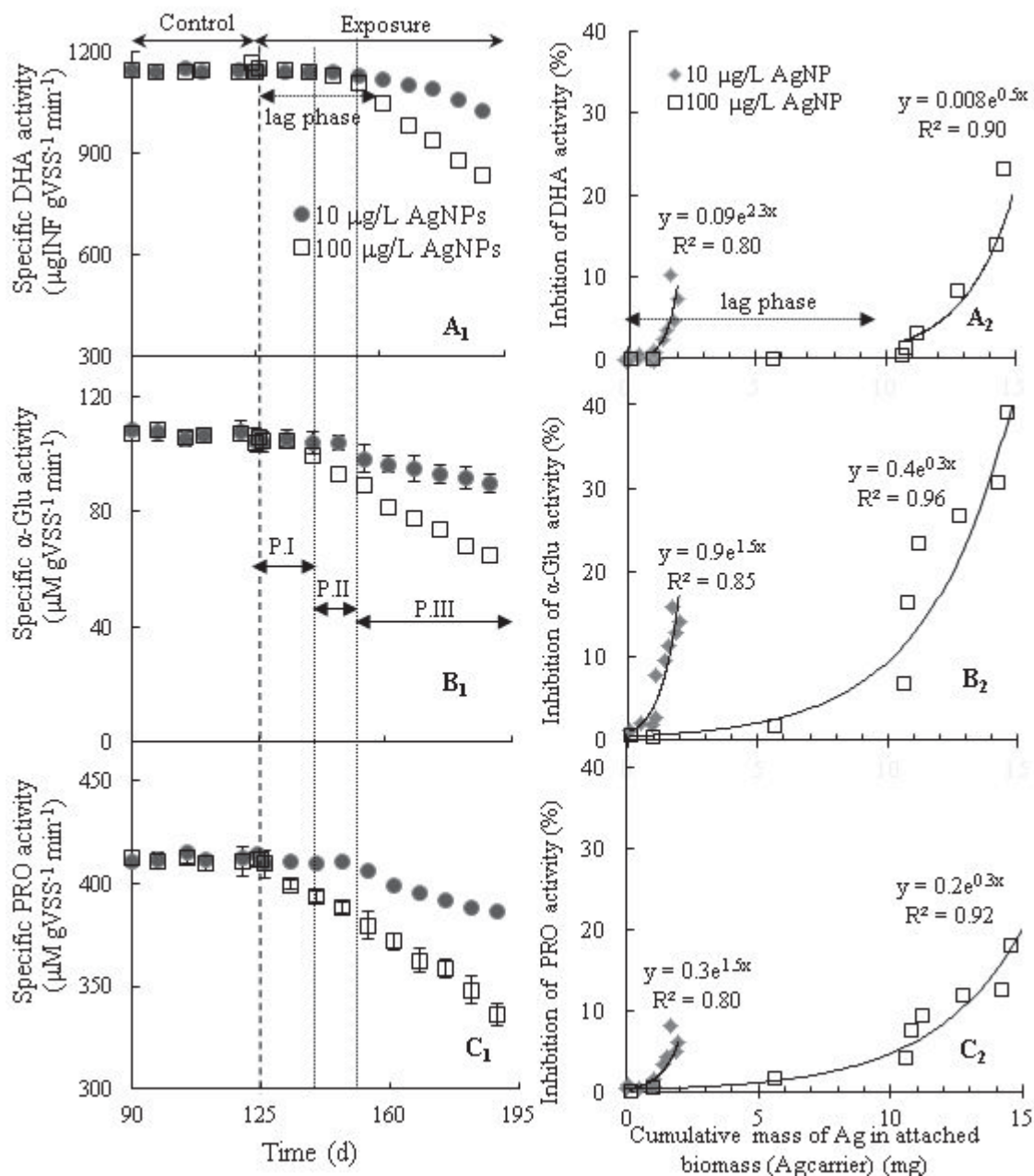
337 Average DHA specific activity was inhibited by about 11% and 27% in MBBR₁ and MBBR₂,
338 respectively, after 64 days (Figure 4A₁). The specific activity of α -Glu and PRO were reduced by
339 $16\% \pm 2\%$ and $8\% \pm 1\%$, respectively, in MBBR₁. Higher enzyme activity inhibitions, up to 39%
340 $\pm 2\%$ (α -Glu) and $18\% \pm 2\%$ (PRO), were observed at higher [AgNP_{inf}] in MBBR₂ (Figure 4B₁,
341 C₁), indicating a dose-dependent effect of AgNPs on specific enzymatic activities of
342 biofilms^{45,486}. Significantly different inhibition rates and half-lives of all three enzymes upon
343 exposure to AgNPs (Table S4) indicated the distinct sensitivity of these enzymes to AgNPs due
344 to their different properties and location patterns in the biofilm matrix⁴⁷.

345 The inhibitory effects of AgNPs on specific enzymatic activities of biofilm was highly correlated
346 ($0.80 < R^2 < 0.96$) to the retained mass of Ag in the carriers ($Ag_{carrier}$) (Figure 4A₂-C₂). The
347 observed pattern highlights the major role of diffusion of retained AgNPs in the biofilm-laden
348 system upon the targeted delivery of both AgNPs and dissolved Ag in close proximity of
349 enzymes and possibly inside the cell in order to reach the Ag concentration needed to exceed
350 inhibitory limits.

351 Upon the initial contact with enzymes in the biological media, nanoparticles acquire a protein
352 corona leading to substantial structural changes of the enzyme⁴⁸. Extracellular enzymes (e.g. α -
353 Glu) interact initially via their functional groups (e.g. carboxyl, hydroxyl, amine, amido, keto)
354 with both the ring and polyvinyl domain of PVP coating and the oxygen atom involved in PVP-
355 nanoparticle complex form. The strong bonding of AgNPs and dissolved Ag with electron
356 donors containing sulfur, oxygen, or nitrogen (e.g. thiols, carboxylates, phosphates, hydroxyl,
357 amines, imidazoles, indoles) across the enzymes can form silver complexes which shield the
358 active sites and alter the enzyme's conformation or distort its 3D structure so it no longer retains
359 its full enzymatic activity⁴⁹. Breaking through the barrier of outer membrane permeability,
360 AgNPs and dissolved Ag can strongly associate with specific sequences of amino acids on the
361 DHA active site and thiol ($-SH$) group of cysteine, by replacing the hydrogen atom to form $-S-$
362 Ag, and irreversibly inactivate dehydrogenase enzymatic functions leading to cellular respiration
363 inhibition^{49,50}. Moreover, the ROS-mediated protein oxidation and microbial community
364 composition alteration can result in loss of function for enzymes associated with biofilms and in
365 a cutback in their production and secretion⁴⁷.

366

367



368

369 **Figure 4.** Effect of continuous PVP-AgNP injection on specific activity of (A₁) DHA (B₁) α-Glu
 370 and (C₁) PRO, (A₂-C₂) correlation between Ag_{carrier} and enzyme activity inhibition (Error bars
 371 are only shown when larger than symbol size).

372

373 3.4 Effects of AgNPs on the microbial community of the heterotrophic wastewater biofilm

374 Seven major phyla (*Proteobacteria*, *Bacteroidetes*, *Verrucomicrobia*, *Gemmatimonadetes*

375 *Planctomycetes*, *Actinobacteria*) were identified (abundance > 1%) at the end of the control

376 period in both reactors (MBBR₁^C, MBBR₂^C) (Figure 5A), as previously reported in microbial
377 composition wastewater biofilm studies^{51,52}. *Proteobacteria* was the most abundant phylum
378 majorly comprised of *Alphaproteobacteria*, *Betaproteobacteria* and *Gammaproteobacteria*.
379 Certain phyla demonstrated a distinct behavior at two [AgNP_{inf}] after 64 days of exposure (day
380 189). The relative abundance of *Proteobacteria* decreased at lower doses of AgNPs (MBBR₁⁶⁴)
381 but increased at the higher dose of AgNPs (MBBR₂⁶⁴) in contrast to *Verrucomicrobia* (Figure
382 5A). AgNPs influenced biofilm microbial phylum abundance in a dose-dependent manner, which
383 was confirmed by the principal coordinate analysis (PCoA) based on the weighted UniFrac
384 distance matrix with 75% of total variance on PCoA1 axis (Figure S6). The observed pattern
385 indicated various responses among taxa, including a range from susceptibility towards silver
386 (e.g. *Bacteroidetes* and *Gemmatimonadetes*) to tolerance against silver (e.g. *Planctomycetes*), as
387 reported in previous studies^{53,54}.

388 The heatmap of genera, with total sequence reads higher than 150 in selected phyla, showed the
389 distinct sensitivity of certain genera at both [AgNP_{inf}] (Figure 5B). The relative abundance of
390 *Rhodobacter*, identified as the most abundant OTU at the genus level (*Rhodobacteraceae*, *α*-
391 *proteobacteria*) decreased in both reactors. Higher abundance of *Paracoccus* other dominant
392 genera from the *Rhodobacteraceae* family and *Zooglea* (*β*-*proteobacteria*) at higher [AgNP_{inf}], is
393 likely associated with their heavy metal resistance to enhance their survival in metal-
394 contaminated environments⁵⁵. The abundance of *Sphingomonas* genus (*Sphingomonadaceae*)
395 decreased in MBBR₁⁶⁴ whereas its abundance increased in MBBR₂⁶⁴, possibly due to the
396 presence of signaling molecules (e.g. sphingolipids) in their outer membrane maintaining
397 community diversity at higher silver concentrations⁵⁶. The genera affiliated with
398 *Xanthomonadaceae* family such as *Stenotrophomona* (*γ*-*proteobacteria*) are reported as N-acyl-

399 homoserine-lactone (AHL) producers in aerobic granular sludge and biofilm, contributing to
400 AHL-mediated quorum sensing signaling, integrity and biofilm stability⁵⁷. Thus, the reduction in
401 their relative abundance at both [AgNP_{inf}] affected both COD removal efficiency and integrity of
402 biofilm structures.

403 Chronic exposure to both [AgNP_{inf}] greatly decreased the relative abundance of genera affiliated
404 to three dominant orders in the *Bacteroidetes* phylum (*Sphingobacteriales*, *Flavobacteriales*,
405 *Cytophagales*) known as the core members of microbial communities in WRRFs degrading
406 complex organic materials⁵⁸, resulting in reduced abundance of *Bacteroidetes* and a correlated
407 lower COD removal efficiency in both reactors. Similar differential susceptibilities to AgNPs
408 were observed in other identified phyla with a shift towards silver-tolerant genera (e.g.
409 *Gemmata*) or more sensitive genera (e.g. *Gemmatimonas*). Although the alpha diversity of the
410 bacterial community was not significantly impacted (Table S4), the bacterial community
411 composition was clearly changed, as shown in Figure 5B, due to a decrease or loss of silver-
412 sensitive species in certain orders (e.g. *Burkholderiales* or *Gemmatimonadales*). The observed
413 shift in the microbial community composition can trigger a potential impairment of the biofilm
414 biological functions pertaining to organic matter biodegradation, enzymatic activities and biofilm
415 structural properties.

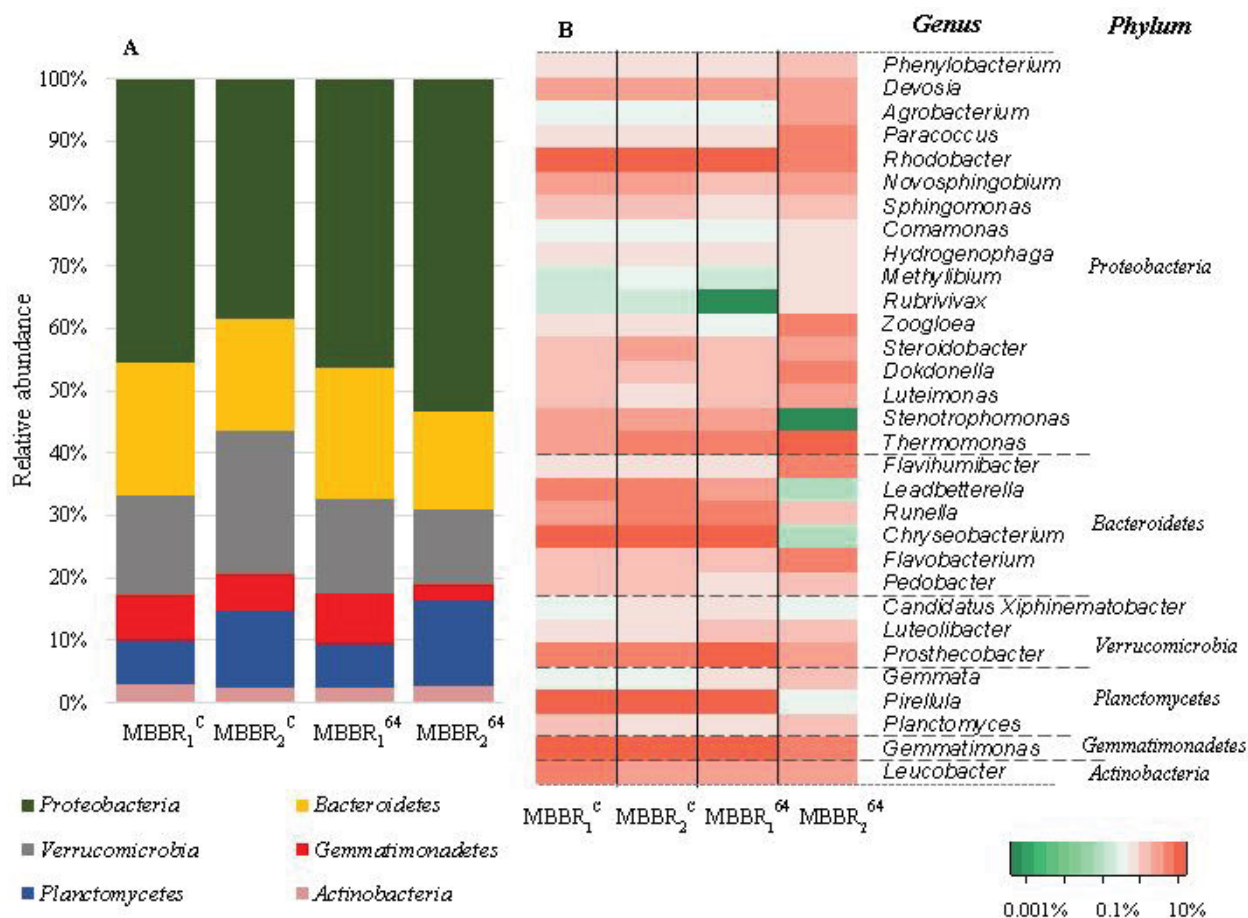
416

417

418

419

420



421

422

423 **Figure 5.** (A) Taxonomic classification of 16S rDNA paired-end sequencing from the biofilm
 424 samples at different AgNP concentrations at phylum level and (B) heatmap of genera with total
 425 sequence reads higher than 150 in selected phyla. Note: Superscripts C and 64 represent the
 426 biofilms collected at the end of control period and after 64 days of AgNPs exposure in MBBRs,
 427 respectively.

428

429 4. Environmental implications

430 The MBBR technology has been successfully used for the treatment of many types of
 431 wastewaters from municipalities, paper mills, pharmaceutical industries and fish farms⁵⁹.
 432 MBBRs can be easily combined with other pre- or post- treatment technologies such as settling
 433 and membrane separation, or used in a series of aerobic and anaerobic MBBRs, thus increasing
 434 the likelihood of achieving a ‘zero discharge’ goal⁶⁰. Our findings, however, suggests that the

435 extended release of AgNPs and Ag-rich biofilm from an MBBR can exert a strong effect on
436 downstream treatments that may lead to membrane fouling, for example, due to significant
437 biofilm detachment, or to potential risks in effluent receiving streams that could impact ecosystems.
438 Our results, corroborated with previous studies^{18,52}, signify that short-term exposure tests may
439 underestimate the inhibitory effects of AgNPs in biofilm-laden environments, especially for
440 treatment processes with long sludge retention times where long-term continuous exposure to
441 AgNPs can result in a cumulative effect of NP-biofilm interaction dynamics leading to a
442 different level of NP-mediated susceptibility in the biofilm. For example, there was no
443 sulfidation of AgNPs in these MBBRs deployed here, due to lack of sulfur in the synthetic
444 wastewater. Sulfidation of AgNPs has been shown to retard dissolution of AgNP due to
445 formation of Ag₂S and organosulfur complexes and could have displayed less^{23,61}.

446 ASSOCIATED CONTENT

447 Supporting Information

448 Additional information is provided for synthetic wastewater composition (Table S1-2) and
449 reactor operational conditions, characterization of biofilm biological responses, intracellular
450 ROS measurements, sp-ICP-MS instrumentation (Table S3) and TEM-EDS, cumulative total Ag
451 mass balance calculations, biofilm enzyme's half-life and inhibition rates (Table S4), richness
452 and diversity of microbial communities of biofilm (Table S5). In addition, fractionation of Ag in
453 reactor components are provided (Figure S1), Ag_{inf/bio} time distribution (Figure S2), AgNP_{inf/eff}
454 particle size distribution (Figure S3), TEM images and EDS analysis for AgNP_{inf/eff} (Figure S4),
455 effluent TSS profile (Figure S5) and principal coordinate analysis (Figure S6) and additional
456 discussion on microbial community analysis.

457

458 Acknowledgements

459 The authors thank the Natural Sciences and Engineering Research Council of Canada (Grant no.
460 STPGP 430659-12), Environment and Climate Change Canada, PerkinElmer, Health Sciences
461 Canada, the Fonds de Recherche du Québec Nature et Technologies (FRQNT), the Canadian
462 Water Network (CWN), SNC Lavalin Environment, the City of Calgary and the City of Saint-
463 Hyacinthe for their financial support. The authors thank Jean-Philippe Massé, Le Centre de
464 Caractérisation Microscopique des Matériaux of Polytechnique Montreal for TEM/EDS analysis,
465 and Jean-Baptiste Burnet for DNA extraction and the Terrebonne/Mascouche WRRF for
466 assistance with wastewater sampling.

467 **References**

- 468
- 469 1. Vance, M. E.; Kuiken, T.; Vejerano, E. P.; McGinnis, S. P.; Hochella Jr, M. F.;
470 Rejeski, D.; Hull, M. S., Nanotechnology in the real world: Redeveloping the
471 nanomaterial consumer products inventory. *Beilstein J. Nanotechnol.* **2015**, *6*, 1769.
- 472 2. Gottschalk, F.; Sonderer, T.; Scholz, R. W.; Nowack, B., Modeled environmental
473 concentrations of engineered nanomaterials (TiO₂, ZnO, Ag, CNT, fullerenes) for
474 different regions. *Environ. Sci. Technol.* **2009**, *43*, (24), 9216-9222.
- 475 3. Keller, A. A.; Lazareva, A., Predicted releases of engineered nanomaterials: From
476 global to regional to local. *Environ. Sci. Technol. Let.* **2013**, *1*, (1), 65-70.
- 477 4. Li, L.; Hartmann, G.; Döblinger, M.; Schuster, M., Quantification of nanoscale silver
478 particles removal and release from municipal wastewater treatment plants in Germany.
479 *Environ. Sci. Technol.* **2013**, *47*, (13), 7317-7323.
- 480 5. Alito, C. L.; Gunsch, C. K., Assessing the effects of silver nanoparticles on biological
481 nutrient removal in bench-scale activated sludge sequencing batch reactors. *Environ.*
482 *Sci. Technol.* **2014**, *48*, (2), 970-976.
- 483 6. Yuan, Z.-H.; Yang, X.; Hu, A.; Yu, C.-P., Long-term impacts of silver nanoparticles in
484 an anaerobic–anoxic–oxic membrane bioreactor system. *Chem. Eng. J.* **2015**, *276*, 83-
485 90.
- 486 7. Zhang, Z.; Gao, P.; Li, M.; Cheng, J.; Liu, W.; Feng, Y., Influence of silver
487 nanoparticles on nutrient removal and microbial communities in SBR process after
488 long-term exposure. *Sci. Total Environ.* **2016**, *569*, 234-243.
- 489 8. Liang, Z.; Das, A.; Hu, Z., Bacterial response to a shock load of nanosilver in an
490 activated sludge treatment system. *Water Res.* **2010**, *44*, (18), 5432-5438.
- 491 9. Sheng, Z.; Van Nostrand, J. D.; Zhou, J.; Liu, Y., Contradictory effects of silver
492 nanoparticles on activated sludge wastewater treatment. *J.Hazard. Mater.* **2018**, *341*,
493 448-456.
- 494 10. Falletti, L.; Conte, L., Upgrading of activated sludge wastewater treatment plants with
495 hybrid moving-bed biofilm reactors. *Ind. Eng. Chem. Res.* **2007**, *46*, (21), 6656-6660.
- 496 11. Walden, C.; Zhang, W., Bioaccumulation of silver nanoparticles in model wastewater
497 biofilms. *Environ. Sci.: Water Res. Technol.* **2018**.
- 498 12. Borkar, R.; Gulhane, M.; Kotangale, A., Moving bed biofilm reactor—a new
499 perspective in wastewater treatment.. *Toxicology and Food Technology* **2013**, *6*, (6),
500 15-21.
- 501 13. Biswas, K.; Taylor, M. W.; Turner, S. J., Successional development of biofilms in
502 moving bed biofilm reactor (MBBR) systems treating municipal wastewater. *Appl.*
503 *Microbiol. Biot.* **2014**, *98*, (3), 1429-1440.
- 504 14. Fabrega, J.; Renshaw, J. C.; Lead, J. R., Interactions of silver nanoparticles with
505 *Pseudomonas putida* biofilms. *Environ. Sci. Technol.* **2009**, *43*, (23), 9004-9009.
- 506 15. Fabrega, J.; Zhang, R.; Renshaw, J. C.; Liu, W.-T.; Lead, J. R., Impact of silver
507 nanoparticles on natural marine biofilm bacteria. *Chemosphere* **2011**, *85*, (6), 961-966.
- 508 16. Mallevre, F.; Fernandes, T. F.; Aspray, T. J., *Pseudomonas putida* biofilm dynamics
509 following a single pulse of silver nanoparticles. *Chemosphere* **2016**, *153*, 356-364.
- 510 17. Peulen, T.-O.; Wilkinson, K. J., Diffusion of nanoparticles in a biofilm. *Environ. Sci.*
511 *Technol.* **2011**, *45*, (8), 3367-3373.

- 512 18. Barker, L.; Giska, J.; Radniecki, T.; Semprini, L., Effects of short-and long-term
513 exposure of silver nanoparticles and silver ions to *Nitrosomonas europaea* biofilms
514 and planktonic cells. *Chemosphere* **2018**, *206*, 606-614.
- 515 19. Alizadeh, S.; Ghoshal, S.; Comeau, Y., Fate and inhibitory effect of silver
516 nanoparticles in high rate moving bed biofilm reactors. *Sci. Total Environ.* **2019**, *647*,
517 1199-1210.
- 518 20. Walden, C.; Zhang, W., Biofilms versus activated sludge: considerations in metal and
519 metal oxide nanoparticle removal from wastewater. *Environ. Sci. Technol.* **2016**, *50*,
520 (16), 8417-8431.
- 521 21. Merrifield, R. C.; Stephan, C.; Lead, J., Determining the concentration dependent
522 transformations of Ag nanoparticles in complex media: Using SP-ICP-MS and Au@
523 Ag core-shell nanoparticles as tracers. *Environ. Sci. Technol.* **2017**, *51*, (6), 3206-
524 3213.
- 525 22. Vidmar, J.; Oprčkal, P.; Milačič, R.; Mladenovič, A.; Ščančar, J., Investigation of the
526 behaviour of zero-valent iron nanoparticles and their interactions with Cd²⁺ in
527 wastewater by single particle ICP-MS. *Sci. Total Environ.* **2018**, *634*, 1259-1268.
- 528 23. Azodi, M.; Sultan, Y.; Ghoshal, S., Dissolution behavior of silver nanoparticles and
529 formation of secondary silver nanoparticles in municipal wastewater by single-particle
530 ICP-MS. *Environ. Sci. Technol.* **2016**, *50*, (24), 13318-13327.
- 531 24. Mitrano, D. M.; Barber, A.; Bednar, A.; Westerhoff, P.; Higgins, C. P.; Ranville, J. F.,
532 Silver nanoparticle characterization using single particle ICP-MS (SP-ICP-MS) and
533 asymmetrical flow field flow fractionation ICP-MS (AF4-ICP-MS). *J. Anal. Atom.*
534 *Spectrom.* **2012**, *27*, (7), 1131-1142.
- 535 25. Pace, H. E.; Rogers, N. J.; Jarolimek, C.; Coleman, V. A.; Gray, E. P.; Higgins, C. P.;
536 Ranville, J. F., Single particle inductively coupled plasma-mass spectrometry: a
537 performance evaluation and method comparison in the determination of nanoparticle
538 size. *Environ. Sci. Technol.* **2012**, *46*, (22), 12272-12280.
- 539 26. Giese, B.; Klaessig, F.; Park, B.; Kaegi, R.; Steinfeldt, M.; Wigger, H.; Gleich, A.;
540 Gottschalk, F., Risks, release and concentrations of engineered nanomaterial in the
541 environment. *Sci. Rep.* **2018**, *8*, (1), 1565.
- 542 27. Metcalf & Eddy-AECOM, Wastewater Engineering: Treatment and Resource
543 Recovery. 5th ed., McGraw-Hill, New York, **2014**.
- 544 28. APHA; AWWA; WEF. Standard Methods for the Examination of Water and
545 Wastewater, 22nd ed. American Public Health Association, American Water Works
546 Association & Water Environment Federation: Washington, D.C. **2012**.
- 547 29. Chen, Y.; Chen, H.; Zheng, X.; Mu, H., The impacts of silver nanoparticles and silver
548 ions on wastewater biological phosphorous removal and the mechanisms. *J. Hazard.*
549 *Mater.* **2012**, *239*, 88-94.
- 550 30. Von Mersi, W.; Schinner, F., An improved and accurate method for determining the
551 dehydrogenase activity of soils with iodinitrotetrazolium chloride. *Biol. Fert. Soils*
552 **1991**, *11*, (3), 216-220.
- 553 31. Goel, R.; Mino, T.; Satoh, H.; Matsuo, T., Enzyme activities under anaerobic and
554 aerobic conditions in activated sludge sequencing batch reactor. *Water Res.* **1998**, *32*,
555 (7), 2081-2088.

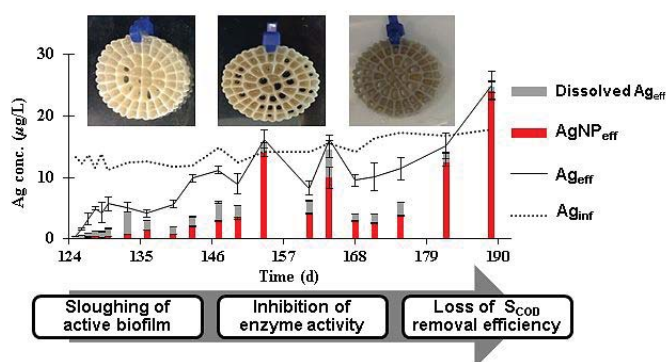
- 556 32. Gu, L.; Li, Q.; Quan, X.; Cen, Y.; Jiang, X., Comparison of nanosilver removal by
557 flocculent and granular sludge and short-and long-term inhibition impacts. *Water Res.*
558 **2014**, *58*, 62-70.
- 559 33. Callahan, B. J.; McMurdie, P. J.; Rosen, M. J.; Han, A. W.; Johnson, A. J.; Holmes, S.
560 P., DADA2: High-resolution sample inference from Illumina amplicon data. *Nat.*
561 *Methods* **2016**, *13*, (7), 581-3.
- 562 34. Lin, S.; Cheng, Y.; Liu, J.; Wiesner, M. R., Polymeric coatings on silver nanoparticles
563 hinder autoaggregation but enhance attachment to uncoated surfaces. *Langmuir* **2012**,
564 *28*, (9), 4178-4186.
- 565 35. Herrling, M. P.; Lackner, S.; Tatti, O.; Guthausen, G.; Delay, M.; Franzreb, M.; Horn,
566 H., Short and long term biosorption of silica-coated iron oxide nanoparticles in
567 heterotrophic biofilms. *Sci. Total Environ.* **2016**, *544*, 722-729.
- 568 36. Kaegi, R.; Voegelin, A.; Ort, C.; Sinnet, B.; Thalmann, B.; Krismer, J.; Hagedorfer,
569 H.; Elumelu, M.; Mueller, E., Fate and transformation of silver nanoparticles in urban
570 wastewater systems. *Water Res.* **2013**, *47*, (12), 3866-3877.
- 571 37. Zhang, C.; Liang, Z.; Hu, Z., Bacterial response to a continuous long-term exposure of
572 silver nanoparticles at sub-ppm silver concentrations in a membrane bioreactor
573 activated sludge system. *Water Res.* **2014**, *50*, 350-358.
- 574 38. Gondikas, A. P.; Morris, A.; Reinsch, B. C.; Marinakos, S. M.; Lowry, G. V.; Hsu-
575 Kim, H., Cysteine-induced modifications of zero-valent silver nanomaterials:
576 implications for particle surface chemistry, aggregation, dissolution, and silver
577 speciation. *Environ. Sci. Technol.* **2012**, *46*, (13), 7037-7045.
- 578 39. Ho, C. M.; Yau, S. K. W.; Lok, C. N.; So, M. H.; Che, C. M., Oxidative dissolution of
579 silver nanoparticles by biologically relevant oxidants: a kinetic and mechanistic study.
580 *Chemistry—An Asian Journal* **2010**, *5*, (2), 285-293.
- 581 40. Azimzada, A.; Tufenkji, N.; Wilkinson, K. J., Transformations of silver nanoparticles
582 in wastewater effluents: links to Ag bioavailability. *Environ. Sci.: Nano* **2017**, *4*, (6),
583 1339-1349.
- 584 41. Yang, Y.; Alvarez, P. J., Sublethal concentrations of silver nanoparticles stimulate
585 biofilm development. *Environ. Sci. Technol. Lett.* **2015**, *2*, (8), 221-226.
- 586 42. Hsiao, I.-L.; Hsieh, Y.-K.; Wang, C.-F.; Chen, I.-C.; Huang, Y.-J., Trojan-horse
587 mechanism in the cellular uptake of silver nanoparticles verified by direct intra-and
588 extracellular silver speciation analysis. *Environ. Sci. Technol.* **2015**, *49*, (6), 3813-
589 3821.
- 590 43. Abdal Dayem, A.; Hossain, M. K.; Lee, S. B.; Kim, K.; Saha, S. K.; Yang, G.-M.;
591 Choi, H. Y.; Cho, S.-G., The role of reactive oxygen species (ROS) in the biological
592 activities of metallic nanoparticles. *Int. J. Mol. Sci.* **2017**, *18*, (1), 120.
- 593 44. Birben, E.; Sahiner, U. M.; Sackesen, C.; Erzurum, S.; Kalayci, O., Oxidative stress
594 and antioxidant defense. *World Allergy Organization Journal* **2012**, *5*, (1), 9.
- 595 45. Asadishad, B.; Chahal, S.; Akbari, A.; Cianciarelli, V.; Azodi, M.; Ghoshal, S.;
596 Tufenkji, N., Amendment of agricultural soil with metal nanoparticles: Effects on soil
597 Enzyme activity and microbial community composition. *Environ. Sci. Technol.* **2018**,
598 *52*(4), 1908-1918.
- 599 46. Xu, Q.; Li, S.; Wan, Y.; Wang, S.; Ma, B.; She, Z.; Guo, L.; Gao, M.; Zhao, Y.; Jin,
600 C., Impacts of silver nanoparticles on performance and microbial community and

- enzymatic activity of a sequencing batch reactor. *J. Environ. Manage.* **2017**, *204*, 667-673.
47. Schug, H.; Isaacson, C. W.; Sigg, L.; Ammann, A. A.; Schirmer, K., Effect of TiO₂ nanoparticles and UV radiation on extracellular enzyme activity of intact heterotrophic biofilms. *Environ. Sci. Technol.* **2014**, *48*, (19), 11620-11628.
48. Ahlberg, S.; Antonopoulos, A.; Diendorf, J.; Dringen, R.; Epple, M.; Flöck, R.; Goedecke, W.; Graf, C.; Haberl, N.; Helmlinger, J., PVP-coated, negatively charged silver nanoparticles: A multi-center study of their physicochemical characteristics, cell culture and in vivo experiments. *Beilstein J. Nanotech.* **2014**, *5*, 1944.
49. Wigginton, N. S.; De Titta, A.; Piccapietra, F.; Dobias, J.; Nesatyy, V.; Suter, M. J.; Bernier-Latmani, R., Binding of silver nanoparticles to bacterial proteins depends on surface modifications and inhibits enzymatic activity. *Environ. Sci. Technol.* **2010**, *44*(6), 2163-2168.
50. Kim, J. Y.; Lee, C.; Cho, M.; Yoon, J., Enhanced inactivation of *E. coli* and MS-2 phage by silver ions combined with UV-A and visible light irradiation. *Water Res.* **2008**, *42*, (1), 356-362.
51. Miao, L.; Wang, C.; Hou, J.; Wang, P.; Ao, Y.; Li, Y.; Yao, Y.; Lv, B.; Yang, Y.; You, G., Response of wastewater biofilm to CuO nanoparticle exposure in terms of extracellular polymeric substances and microbial community structure. *Sci. Total Environ.* **2017**, *579*, 588-597.
52. Wang, P.; You, G.; Hou, J.; Wang, C.; Xu, Y.; Miao, L.; Feng, T.; Zhang, F., Responses of wastewater biofilms to chronic CeO₂ nanoparticles exposure: Structural, physicochemical and microbial properties and potential mechanism. *Water Res.* **2018**, *133*, 208-217.
53. Grün, A. Y.; App, C. B.; Breidenbach, A.; Meier, J.; Metreveli, G.; Schaumann, G. E.; Manz, W., Effects of low dose silver nanoparticle treatment on the structure and community composition of bacterial freshwater biofilms. *PLoS one* **2018**, *13*, (6), e0199132.
54. Cao, C.; Huang, J.; Yan, C.; Liu, J.; Hu, Q.; Guan, W., Shifts of system performance and microbial community structure in a constructed wetland after exposing silver nanoparticles. *Chemosphere* **2018**, *199*, 661-669.
55. Zheng, X.-y.; Lu, D.; Chen, W.; Gao, Y.-j.; Zhou, G.; Zhang, Y.; Zhou, X.; Jin, M.-Q., Response of aerobic granular sludge to the long-term presence of CuO NPs in A/O/A SBRs: Nitrogen and phosphorus removal, enzymatic activity, and the microbial community. *Environ. Sci. Technol.* **2017**, *51*, (18), 10503-10510.
56. Yang, Y.; Quensen, J.; Mathieu, J.; Wang, Q.; Wang, J.; Li, M.; Tiedje, J. M.; Alvarez, P. J., Pyrosequencing reveals higher impact of silver nanoparticles than Ag⁺ on the microbial community structure of activated sludge. *Water Res.* **2014**, *48*, 317-325.
57. Tan, C. H.; Koh, K. S.; Xie, C.; Tay, M.; Zhou, Y.; Williams, R.; Ng, W. J.; Rice, S. A.; Kjelleberg, S., The role of quorum sensing signalling in EPS production and the assembly of a sludge community into aerobic granules. *The ISME journal* **2014**, *8*, (6), 1186.
58. Chen, Y.; Zhao, Z.; Peng, Y.; Li, J.; Xiao, L.; Yang, L., Performance of a full-scale modified anaerobic/anoxic/oxic process: high-throughput sequence analysis of its microbial structures and their community functions. *Bioresour. Technol.* **2016**, *220*, 225-232.

- 647 59. Revilla, M.; Galán, B.; Viguri, J. R., An integrated mathematical model for chemical
 648 oxygen demand (COD) removal in moving bed biofilm reactors (MBBRs) including
 649 predation and hydrolysis. *Water Res.* **2016**, *98*, 84-97.
- 650 60. Bakar, S. N. H. A.; Hasan, H. A.; Mohammad, A. W.; Abdullah, S. R. S.; Haan, T. Y.;
 651 Ngteni, R.; Yusof, K. M. M., A review of moving-bed biofilm reactor technology for
 652 palm oil mill effluent treatment. *J.Clean. Prod.* **2018**, *171*, 1532-1545.
- 653 61. Levard, C.; Reinsch, B. C.; Michel, F. M.; Oumahi, C.; Lowry, G. V.; Brown Jr, G. E.,
 654 Sulfidation processes of PVP-coated silver nanoparticles in aqueous solution: impact
 655 on dissolution rate. *Environ. Sci. Technol.* **2011**, *45*, (12), 5260-5266.

658 **TABLE OF CONTENT GRAPHIC**

659



677

678

679